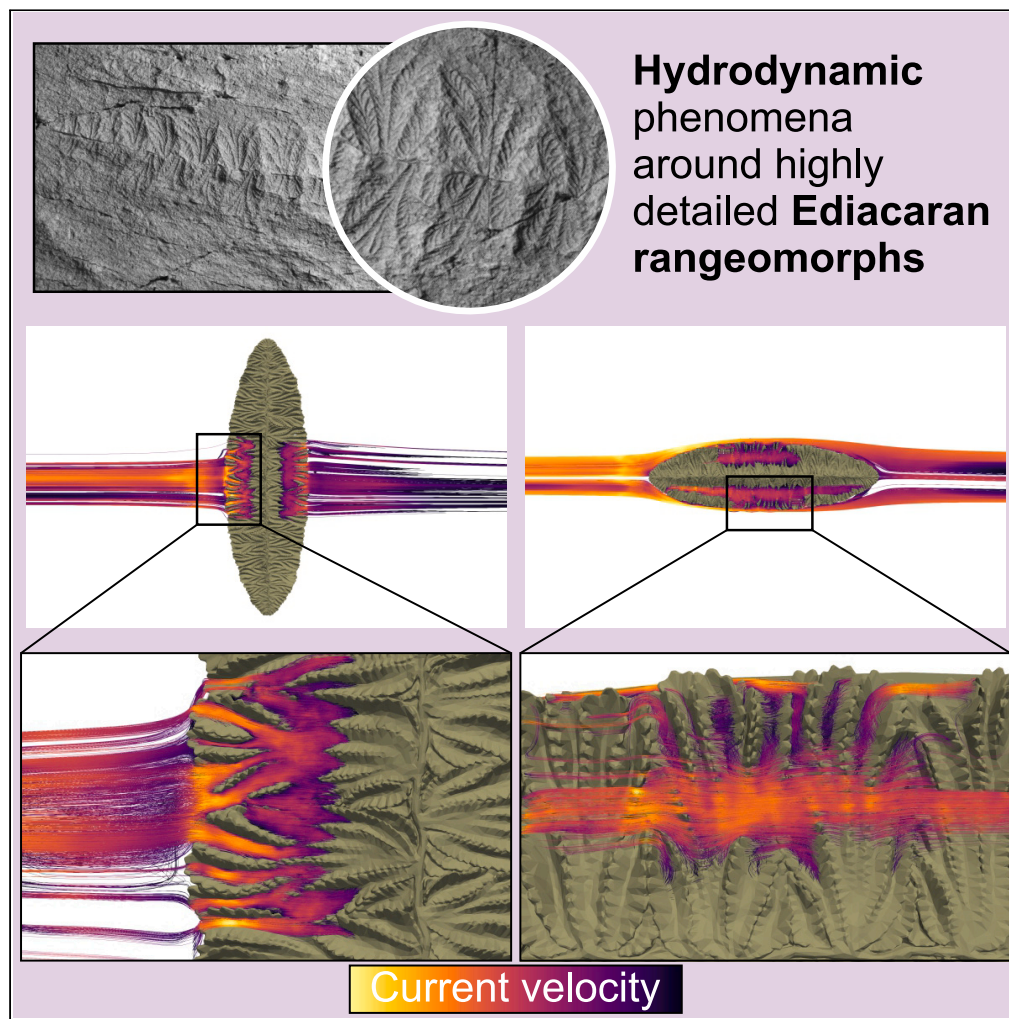


## Article

Hydrodynamic insights into the paleobiology of the Ediacaran rangeomorph *Fractofusus misrai*

Daniel Pérez-Pinedo, Robert Nicholls, Jenna M. Neville, Duncan McIlroy

dperezpinedo@mun.ca

**Highlights**

Hydrodynamic phenomena around *Fractofusus misrai* documented for the first time

Oblique orientations as a trade-off from maximized absorption and reduced drag

Flow patterns support gas exchange, collection POM/DOM, and metabolite flushing

The wake downstream could modify sedimentation patterns on the seafloor

Pérez-Pinedo et al., iScience 27, 110107  
June 21, 2024 © 2024 The Authors. Published by Elsevier Inc.  
<https://doi.org/10.1016/j.isci.2024.110107>

## Article

Hydrodynamic insights into the paleobiology of the Ediacaran rangeomorph *Fractofusus misrai*Daniel Pérez-Pinedo,<sup>1,3,\*</sup> Robert Nicholls,<sup>2</sup> Jenna M. Neville,<sup>1</sup> and Duncan Mcllroy<sup>1</sup>

## SUMMARY

The Ediacaran of Newfoundland preserves some of the oldest complex macroscopic communities, several of which are dominated by the fractal-like rangeomorph genus *Fractofusus*. Here we use computational fluid dynamics and a detailed reconstruction of *Fractofusus misrai* to document for the first time hydrodynamic phenomena associated with this sediment-reclining organism and its rangeomorph elements that are relevant to interpreting feeding strategies, explain the recently documented rheotropic growth oblique to currents, and provide insights into their impact on the Ediacaran seafloor. Obliquely oriented *Fractofusus* are common, likely representing a compromise between maximized aspect ratio and minimization of drag. Flow patterns on the upper surface of *Fractofusus* are consistent with the collection of dissolved and finely particulate nutrients, as well as gas exchange. *Fractofusus* produce a wake downstream, demonstrating that reclining rangeomorphs had potential to modify sedimentation patterns on the ancient seafloor by potentially allowing deposition of fine-grained sediment.

## INTRODUCTION

Fossil assemblages that preserve the soft-bodied Ediacaran biota include the oldest remains of architecturally complex macroscopic life on Earth and therefore are essential in furthering our understanding of the evolution of complex macroorganisms.<sup>1–6</sup> The Avalon Assemblage is the oldest of the Ediacaran assemblages and includes the deep marine volcanoclastic settings of the Avalon Terrane in Newfoundland spanning at least the interval circa 574–564 Ma<sup>5</sup> and Charnwood Forest, UK.<sup>7</sup> The Ediacaran of Newfoundland is largely dominated by the clade Rangeomorpha<sup>8</sup> which is considered to include the oldest examples of stem eumetazoans.<sup>9–12</sup> These organisms are characterized by frondose body plans, pseudo-fractal branching architecture consisting of similar orders of self-repeating branches, and high surface area/volume ratios that are not seen in modern organisms.<sup>8,13</sup> The basic rangeomorph unit can grow in a number of different orientations to create a range of morphologies in the preserved bedding plane expression of the 3D form.<sup>6,8,14,15</sup>

Species of the rangeomorph genus *Fractofusus* (*F. misrai* and *F. andersoni*) are endemic to the offshore to deep basinal Ediacaran facies of the island of Newfoundland<sup>3,16–18</sup> (and putative examples from McKenzie Mountains Canada)<sup>19</sup> where they are found on minor hiatal surfaces in turbiditic successions associated with well-developed matgrounds.<sup>17</sup> *Fractofusus misrai* dominates the D and E surfaces at Mistaken Point<sup>20,21</sup> and the “Melrose Surface” at Capelin Gulch in the Discovery UNESCO Global Geopark.<sup>22</sup> These organisms inhabited deep marine paleoenvironments and are preserved by obrution and smothering beneath volcanic ashes or tuffites.<sup>3,5,23–25</sup>

Early considerations of the mode of feeding in the Rangeomorpha focused on filter feeding by comparison with morphological analogues in the Cnidaria<sup>26</sup> and also through inferences based on the tiered community structure.<sup>20,27</sup> Earlier inferences of suspension feeding (relying on particulate organic matter [POM])<sup>26,27</sup> and absorption of dissolved organic matter (DOM)<sup>13</sup> as the primary mode of feeding in the Rangeomorpha have been contested,<sup>6,8,22,28–30</sup> and phagocytotic/chemosymbiotic feeding at the organism-substrate interface has been proposed for feeding in reclining organisms.<sup>5,30–33</sup> Determining the feeding strategies for rangeomorphs like *Fractofusus* is problematic due to the lack of direct modern analogues,<sup>23</sup> their unique body plan,<sup>8,14</sup> and incomplete (mostly 2D) preservation (but see Narbonne and other studies<sup>34–38</sup>).

While the debate over the mode of life of the Rangeomorpha is ongoing, the mode of life of *Fractofusus* as a sessile epibenthic recliner is widely accepted. Preferential orientation of Ediacaran fronds in the Avalon Assemblage has been interpreted as a result of current alignment due to felling of erect fronds.<sup>23,39</sup> Taphonomic evidence to support erect modes of life in some taxa comes from poorly preserved distal features obscured by the deposition of sediment/tuff in between these features and the preservation plane.<sup>33</sup> However, *Fractofusus* has always been interpreted as a reclining organism lying flat on the seafloor<sup>24,40</sup> supported by their apparently random orientation at Bristy Cove, the E Surface at Mistaken Point Ecological Reserve (MPER), and the Johnson/H14 surface at Discovery Global Geopark<sup>21,30,39–41</sup> and also the ubiquitously well-preserved nature of their lower surface impressions.<sup>18,31</sup> Preferential orientations of *Fractofusus misrai*, oblique to a paleocurrent, have however been reported at Capelin Gulch near Melrose in the Catalina Dome (Figure 1).<sup>22</sup> This fossiliferous surface is significant because paleocurrents at the site can be determined from current ripples associated with the fossiliferous bedding plane.<sup>22</sup> Using Ediacaran

<sup>1</sup>Department of Earth Sciences, Memorial University of Newfoundland, St. John's, NL A1B3X5, Canada

<sup>2</sup>Bob Nicholls Art, Kingswood, Bristol BS15 9QQ, UK

<sup>3</sup>Lead contact

\*Correspondence: dperezpinedo@mun.ca  
<https://doi.org/10.1016/j.isci.2024.110107>



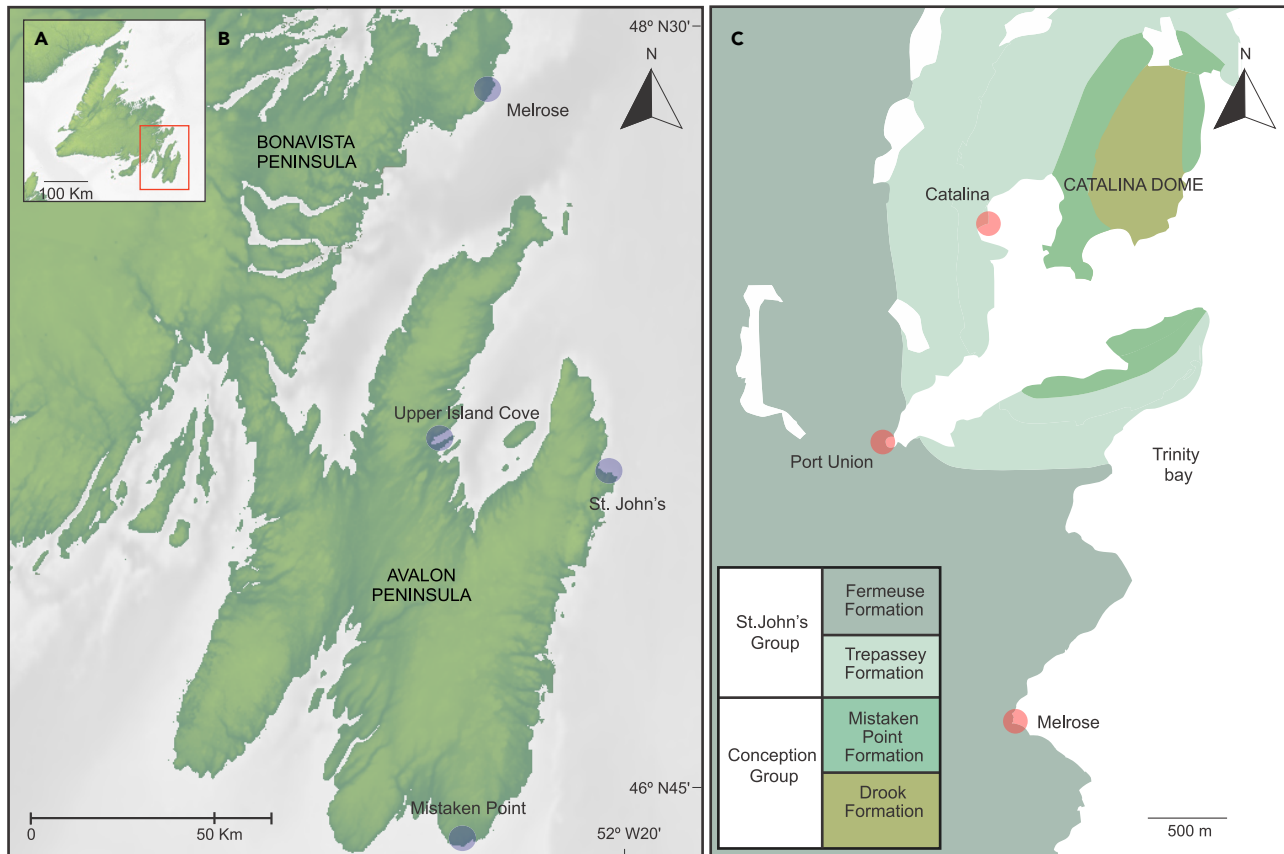


**Figure 1. Location of the Capelin Gulch site, also known as “Melrose Surface” in the Fermusee Formation at Melrose, on the southern portion of the Catalina Dome, in the Discovery UNESCO Global Geopark**

(A) General map of Newfoundland, Atlantic Canada.

(B) Detail of the Avalon and Bonavista Peninsulas.

(C) Geologic map of Catalina area and stratigraphic column.

fossil orientations to infer paleocurrents is problematic owing to debate concerning the mode of life of many frondose taxa, particularly the Rangeomorpha.<sup>30</sup> The determination of non-random *Fractofusus* orientation trends oblique to a paleocurrent at Capelin Gulch poses new questions regarding the paleobiology and paleoecology of *F. misrai* that we address herein (Figure 2).

Computational fluid dynamics (CFD) has been used to understand the feeding strategies of some Ediacaran organisms and to determine their roles in Ediacaran ecosystems. It has been proposed that passive suspension feeders generate patterns of flow recirculation toward feeding structures (e.g., pores) or specific parts of the anatomy creating areas of low velocity facilitating the gravitational deposition of particles. On the other hand, the passive absorption of DOM is related to high surface area (SA)/volume (V) ratios (i.e., fractal branching) and an even, relatively undisturbed, distribution of flow over the entire organism surface.<sup>42–49</sup> However, previous hydrodynamic studies of the Rangeomorpha have not addressed the complex surface morphology of rangeomorphs and have instead focused on gross morphology rather than detailed paleobiological reconstructions.<sup>45</sup> In this study, we present a novel hydrodynamic approach to studying *F. misrai*, integrating the detailed three-dimensional geometry published by Taylor et al.<sup>18</sup> (Figure 3) and the statistically significant orientation groups found by Pérez-Pinedo et al.<sup>22</sup> We aim to document the fluid flow near the reconstructed *F. misrai* relevant to feeding strategies and metabolite collection (cf. Dufour et al. and Darroch et al.<sup>31,45</sup>), analyze the hydrodynamic behavior of preferential orientation clusters (cf. Taylor et al. and Pérez-Pinedo et al.<sup>18,22</sup>), and gain insights into the paleoecology of *F. misrai*.

## RESULTS

### Meshing parameters of the computational domain and the *F. misrai* geometry

The resulting meshes consisted of approximately 2–4 million cells and 500,000–1 million nodes (Figure 3). The final mesh was created using medium global mesh fineness, with 3 prismatic boundary layers, of 0.4 thickness of the local mesh size at a growth rate of 1.5. Physics-based meshing was employed to consider the physics in the simulation setup including refinements at the inlet and outlet

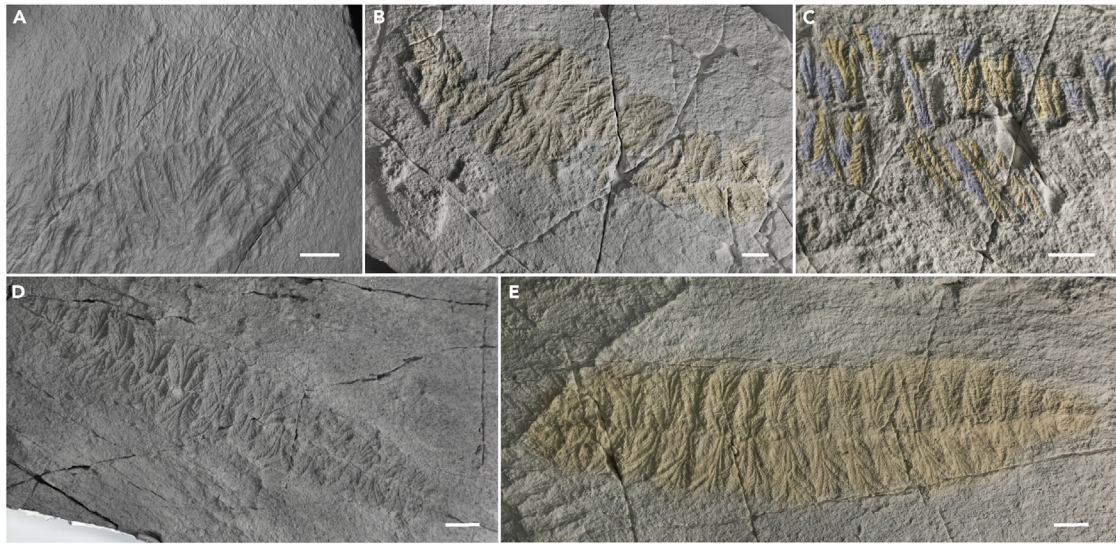


**Figure 2. Taphonomic variability of *Fractofusus misrai* exemplified by specimens from the E Surface at Mistaken Point, NL**

(A) *F. misrai* partially rotated by the current to produce a kink in the axis.

(B) Specimen (yellow) with a branch that has been lifted by the current leaving a triangular gap in the row of rangeomorph branches.

(C) Tightly packed branches in a specimen showing a combination of rangeomorph branches rotated through 90° to show only one row of secondary-order branches (yellow) and unrotated branches with the tips curled away from the bedding plane to produce straight lateral margins (blue).

(D) Largely undisturbed *F. misrai* with displayed tips to the primary-order branches.

(E) Straight margined specimen inferred to have been created by the lifting of the tips of the primary-order branches by a current meaning that they were not in contact with the seafloor at the time of casting. Scale bars 1 cm.

of the flow volume region (FVR). Hexahedral element core was used to fill the inner mesh with hexahedral elements. The conversion from hexahedral to triangulated elements was done using pyramidal and tetrahedral elements. The small feature suppression was set at 0.015 mm, the gap refinement factor at 0.05, and the global gradation rate at 1.22 to guarantee a good resolution. The overall mesh quality (based on the 99.99 percentile) was between 0.035 and 1.0 as indicated by the CFD software, and minimum edge length was  $\sim 0.015$  mm. This captures anatomical details of even third-order branches (0.3 mm) in the smallest *Fractofusus*. Cartesian boxes of  $1 \times 0.5 \times 0.2$  m and 0.01 m maximum edge length were employed to assess the impact of mesh region refinements around the *F. misrai* geometry; however, their use was deemed unnecessary as standard-finite-volume meshing algorithms automatically generated finer meshes in the desired areas based on geometric estimations. Additionally, higher-resolution meshes or region refinements led to increased computational demands without relevant changes in terms of flow patterns and the quantification of forces (Figures S1–S3; Table S1; see *F. misrai* geometry in supplemental information).

### Velocity field and flow recirculation patterns

In all CFD simulations,  $U_x$  decreased on the downstream side of the obstacle, after the fluid encountered the *F. misrai* geometry (Figures 4 and S4–S6). This resulted in the development of a pronounced velocity gradient from the bottom boundary of the flow domain. The thickness of this boundary layer decreased as the inlet velocity increased (cf. Cracknell et al.<sup>48</sup>). Slow-flow regions (wakes) extending approximately 2.5 m in length formed downstream of *F. misrai*. This zone of reduced flow velocity was weaker in the null model simulations (Figure S7). The wake was found to be wider and higher in experiments with 1) slower current velocities and 2) increasing size of *Fractofusus* (Figures 4, S4, and S5). Velocity profiles ( $U_z$ ) were visualized and affirmed the logarithmic law of the wall ensuring fully developed flows by the time the flows encounter the fossil geometry (cf. Gibson et al.<sup>50</sup>; Figure S8).

At a small scale, current-parallel *Fractofusus* show flow retention in the form of funneled flow vortices that are routed toward the axis along the length of the concave grooves of the secondary-order branches. The flow that is entrained into these depressions shows marked reduction in  $U_x$ , starting at the distal end of the branches and progressing toward the midline (Figures 5A–5D and S6). Additionally, weak eddying was found on the lee side of the geometry, which creates potential for lifting of the distal margin of the secondary-order branches (Figure 4Sii). Increasingly perpendicular front orientations show a relatively undisturbed, even distribution of flow at the secondary-order branch-water interface (Figures 5E–5L). This uniform flow is accelerated at the distal end of the upstream branches as it is channeled by the grooves formed by the secondary-order branches. The flow decelerates toward the axis where secondary-order branches are more concave (Figures 5E–5L) and accelerates again on the lee side of the midline (Figure S6). The progressively perpendicular orientations also show minor flow retention manifesting as small and highly constrained vortices parallel to the secondary-order branches on the distal end of the upstream branches and downstream of the midline (Figure 4Tii–Tiii). In addition, enhanced eddying where flow recirculation resulted in velocity pulses against the

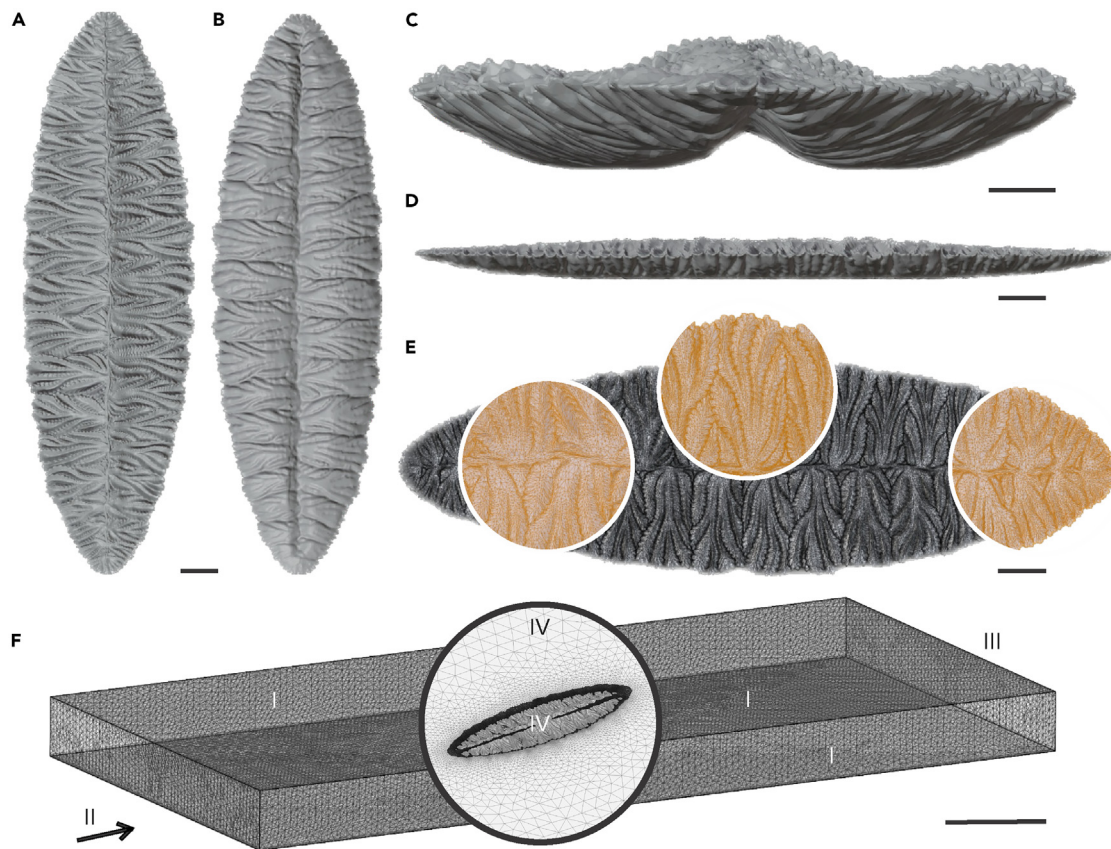


**Figure 3. Digital three-dimensional reconstruction of *Fractofusus misrai* and computational domain**

(A–D) Different perspectives of the *F. misrai* geometry. (A) Top view, (B) bottom view, (C) front view, and (D) lateral view.

(E) *F. misrai* tetrahedral mesh and detail view (zoomed in).

(F) Flow volume region mesh and boundary conditions: I) slip boundary condition, II) velocity inlet, III) pressure outlet, and IV) no-slip boundary condition. Scale bars 2 cm except (C) 1 cm, and (F) 50 cm.

See Figures S1 and S2.

organism (Figure 4Ti, Tiv) formed on both the stoss and lee sides of increasingly current-perpendicular fronds compared to parallel orientations. These flow patterns were observed in all simulations in turbulent flows regardless of flow velocities and organism size (Figures 4, S4, and S5). No flow retention was observed on top of the smooth null models (Figure S7).

### Drag force

Drag force was found to increase with 1) increasing flow velocity, 2) larger *F. misrai* geometries, and 3) increasingly current-perpendicular *Fractofusus* orientations (cf. Darroch et al.<sup>43</sup>; Figure 6; Table S1). In current-parallel orientations, drag-induced high-stress areas were found to be concentrated on both sides of the laterally directed secondary-order branches of *Fractofusus* (Figure 6A). In progressively current-perpendicular orientations, high-stress areas exhibited a more widespread distribution: 1) concentrated along both sides of the midline, 2) following the ridges formed by the secondary-order branches, and 3) associated with the distal portion of both rows of first-order branches (Figures 6B–6D). Final result convergence in all CFD simulations was confirmed by the examination of the residuals, the solution imbalances (close or below  $1e^{-3}$ ), and boundary conditions convergence plots grouped as domain, inlets, outlets, and walls. These show the average values of the studied parameters for every iteration and present them normalized and scaled. This revealed the absence of relevant global or local imbalances (see CFD files in supplemental information; additional results are available upon request).

### DISCUSSION

*Fractofusus misrai* is one of the best known, most abundant, and least contentious elements of the Ediacaran biotas of Newfoundland. Improved understanding of how *Fractofusus* might have interacted with its environment is key to better understanding the paleobiology of the Rangeomorpha as a whole. Our approach of integrating, taphonomy, morphological reconstruction, sedimentological context, and CFD highlights a number of phenomena of note.

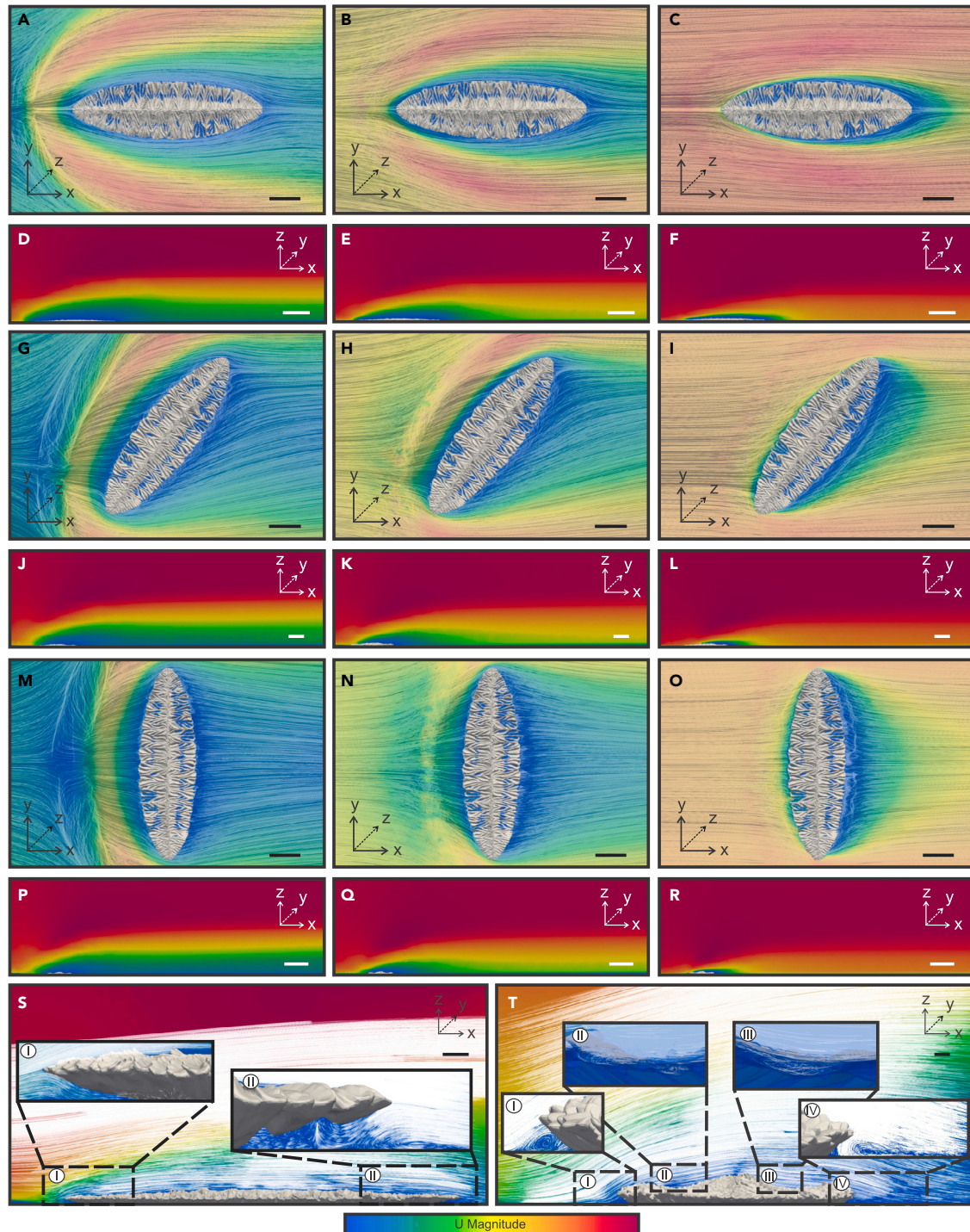


**Figure 4. CFD simulations of large *Fractofusus misrai* in different orientations relative to the simulated flow from (left to right)**

(A–R) Two-dimensional horizontal and cross-sectional surface plots of streamlines and different  $U_x$  regimes: first column (A, D, G, J, M, and P) simulated flow of 0.05 m/s; second column (B, E, H, K, N, and Q) flows of 0.1 m/s; and third column (C, F, I, L, O, and R) 0.2 m/s.

(S and T) Detailed cross-sectional view of flow retention patterns and eddying of current-parallel (Si–Sii) and current-perpendicular *Fractofusus misrai* (Ti–Tiv) in 0.1 m/s flow. Both orientations show the eddying at the frond margin (Si–Sii; Ti, Tiv). Current-perpendicular *F. misrai* also shows weak vortices on the upper surface of the frond both upcurrent of the axis of the frond (Tii), and also in the lee of the axis (Tiii). Velocity ranges from 0 to 0.05, 0.1, or 0.2 m/s as indicated in this caption. Scale bars top view 5 cm, cross-sectional view 10 cm except S, and T 2 cm.

See Figures S3–S5, S7, and S8.

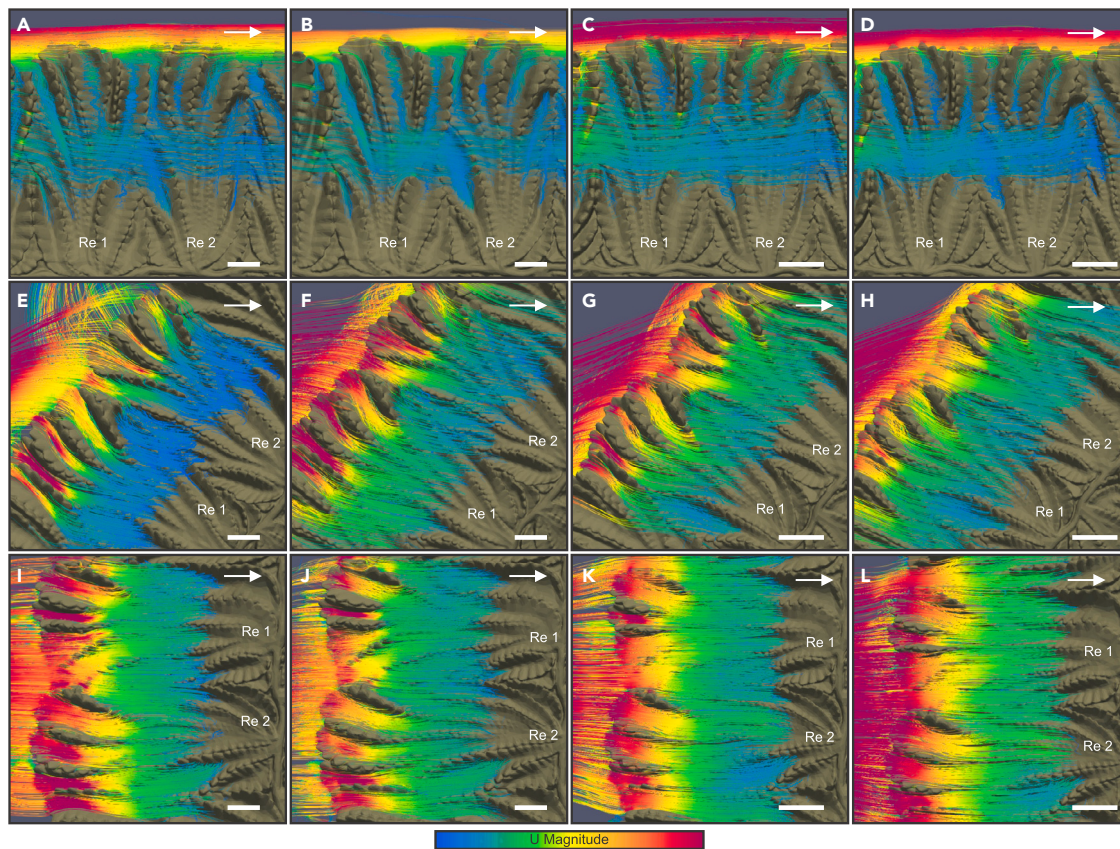


**Figure 5. Detailed top view of flow patterns over the same rangeomorph elements of *Fractofusus misrai* (Re 1 and Re 2) in different orientations relative to the current**

Streamlines vary in their paths between current-parallel and current-oblique/perpendicular orientations but are routed by the surface morphology in all cases. Flow velocity is colored along the streamlines according to velocity (red fastest, blue slowest): (A–D) current-parallel ( $0^\circ$ ), (E–H) current-oblique ( $52^\circ$ ), and (I–L) current-perpendicular ( $90^\circ$ ). (A), (E), and (I) are all the case of a small *F. misrai* under 0.05 m/s flow in different orientations; (B), (F), and (J) are all small *F. misrai* experiencing a 0.1 m/s flow in different orientations. (C), (G), and (K) show the case of large *F. misrai* in a 0.05 m/s flow in different orientations; (D), (H), and (L) show the effects of a large *F. misrai* experiencing a 0.1 m/s flow in different orientations. Current flow from left to right. Velocity ranges from 0 to 0.05, or 0.1 m/s as indicated in this caption. Scale bars 0.1 cm for small and 1 cm for large *F. misrai*.

See Figure S6.

### Feeding strategies

The funneled vortices in the grooves of secondary-order branches in current-parallel *F. misrai* are of benefit to a range of feeding strategies (e.g., suspension feeding and DOM absorption) due to entrainment of flow and irrigation of the upper surface of the organism. The retention of flow within these depressions arises from flow separation over the secondary branches and lateral flow being drawn into the perpendicularly directed grooves (Figures 5A–5D). The slowed flow forms pronounced vortices progressing from the distal end of the branches toward the axis of the organism where it is flushed by the faster overlying ambient current. *Fractofusus* lived in association with very slow currents; further slowing of currents in the grooves may have enhanced active capture of low-density food particles (e.g., very fine POM) on the upper surface of *Fractofusus*. Sediment supply in these low velocity background currents was likely very low and fine grained with no associated erosional or depositional sedimentary structures. The flow velocity over the rangeomorph elements across all modeled scenarios is in the range  $\sim 0.005$ – $0.08$  m/s. Moreover, it has previously been hypothesized that *Fractofusus* could have also relied on ciliated cells to remove small amounts of sediment and to enhance feeding efficiency on the upper surface of the organism.<sup>31</sup> However, caution is required for the interpretation of this phenomenon as it is governed by Archimedes and Froude numbers,<sup>51</sup> and the behavior of very small particles in the flow has not been simulated in this work and the exact means of organic matter collection by ciliated or choanocyte-like cells is not tested either. The potential for using the entire upper surface of *Fractofusus* for capture of organic matter and subsequent phagocytotic ingestion has been previously predicted<sup>31</sup> and invited comparison of the Rangeomorpha with organisms of a pre-sponge grade of organization.<sup>31,52,53</sup> Some previous studies of flow in association with non-rangeomorph Ediacaran organisms have demonstrated the routing of funneled vortices toward particular portions of the organism, which have been inferred to have had unpreserved specialized suspension-feeding organs.<sup>42,43,48</sup> However, invoking suspension-feeding strategies in the Rangeomorpha falls short due to 1) the absence of paleontological evidence for

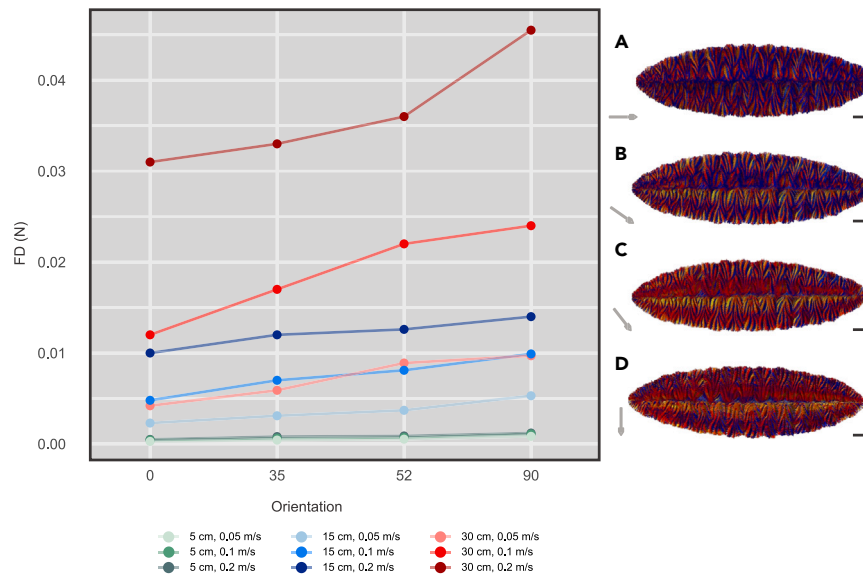


**Figure 6. Drag forces of *Fractofusus misrai* models in CFD simulations**

(A–D) Spatial visualization of drag force in *Fractofusus* oriented: (A) parallel (0°), (B) oblique (35°), (C) oblique (52°), and (D) perpendicular (90°) with respect to the paleocurrent. Arrows indicate the paleocurrent direction. Scale bars 2 cm. Progressively warmer colors represent increasing drag. See to Table S1.

pores or zooids<sup>4,6</sup> (but see Butterfield<sup>54</sup>), 2) flawed anatomical comparisons to the Pennatulacea,<sup>28</sup> 3) the lack of consistent flow recirculation patterns toward specific areas,<sup>45</sup> and 4) disagreements concerning the mode of life of many rangeomorphs, which underpin ecological tiering models that have been used to infer that the Rangeomorpha formed suspension-feeding communities.<sup>22,27,30,45,55</sup>

Oblique orientations of *Fractofusus* relative to a current demonstrate flow retention on the surface of the fronds in the form of minor vortices due to flow separation on the lee side of the distal end of the upstream primary branches and downstream of the midline (Figure 4Tii–Tiii). The flow vortices are weak and tightly constrained to the middle section of the organisms therefore showing very limited potential to aid the vertical mixing of the water column or play a relevant role in feeding efficiency. Flow on the upper surface of *Fractofusus* on both sides of the axis is highly constrained within the concave morphology of the secondary-order branches, resembling a creeping flow, which is channeled by the branches (Figures 5E–5L). On the upcurrent side of the fossil, flow is directed toward the axis showing a progressive reduction in velocity, but on the downcurrent side flow is drawn away from the axis featuring a reverse velocity trend (Figure S6). This disparity in flow direction relative to the axis argues against the presence of food-capturing loci along the midline and instead supports the inference that the whole upper surface of the organism was used to exploit nutrients from the slowed current.<sup>31</sup> The even distribution of relatively undisturbed flow is compatible with the collection of metabolites such as DOM<sup>42,43,48,56</sup> and aligns with the inference of Dufour and McIlroy<sup>31</sup> that, while the lower surface likely harbored chemosymbionts, the upper surface of *Fractofusus* could be used for DOM and/or oxygen uptake. Previous studies hypothesized that (non-rangeomorph) fronds could have been suited for oxygen uptake benefiting from oscillatory behavior of the frond in a current<sup>56</sup> and by reaching faster fluids occurring at greater heights.<sup>55</sup> Following Darroch et al.<sup>45</sup> the high SA/V of *Fractofusus* and the faster flowing fluid over the primary branches might have reduced the thickness of the diffusive boundary layer, thereby improving gas exchange. Eddying observed on the stoss and lee sides of the distal margin of primary branches, which project above the sediment-water interface, is likely to have caused some oscillatory movement of the distal portions of rangeomorph elements resulting in similar dynamics as those observed in arboreomorphs<sup>56</sup> and the erect rangeomorph *Pectinifrons*.<sup>45</sup>

Inferences that rangeomorphs like *Fractofusus* were giant obligate osmotrophs<sup>13</sup> have been challenged on grounds of palaeobiology/morphology,<sup>6,30,54</sup> and also in terms of the concentration of the DOM reservoir of Ediacaran oceans, which is now considered to be too low to have supported obligate osmotrophic macroorganisms.<sup>29,57</sup> Moreover, the SA/V ratios calculated for our geometry (0.31–2.06 mm<sup>-1</sup>; Table S1) are significantly lower than those estimated by Laflamme et al.<sup>13</sup> The pseudo-fractal lower surface of sessile recliners like *F. misrai*<sup>17,23</sup> is considered to be an adaptation to maximize SA in contact with the sediment<sup>31</sup> (Figures 2 and 3B). In the absence of surficial bioturbation<sup>58</sup> a redoxcline would have developed at or close to the sediment-water interface,<sup>59</sup> so the lower surface would have been exposed to the, potentially toxic, buildup of reduced sulfur produced in the underlyingly anoxic pore waters.<sup>6,31</sup> This has led to the suggestion that epibenthic recliners like *F. misrai* may have benefited from symbiotic interactions with, for example, sulfur-oxidizing chemolithoautotrophic bacteria.<sup>6,31</sup> In this scenario, the even oxygen flow along the secondary branches might have been dorsoventrally transported by diffusion through the thin organism, or by ciliary action around the frondlet, to increase the productivity of chemolithoautotrophs both in the underlying porewater system and on the lower surface of the reclining organism. The mode of feeding probably involved a combination of ectosymbiosis and phagocytosis.<sup>31</sup> Given the results shown by the CFD simulations of *F. misrai*, in the context of the orientation trends determined by

Pérez-Pinedo et al.,<sup>22</sup> we support the hypothesis that *F. misrai* could have fed on both particulate and truly dissolved DOM via its upper surface if covered by cilia/choanocytes<sup>52,53</sup> and employed chemosymbiotic strategies on its lower surface, perhaps facultatively changing feeding mode as demonstrated for some chemosymbiotic clams.<sup>60</sup>

### Orientation and drag

The erect mode of life invoked for frondose Ediacaran taxa<sup>26,61</sup> has recently been challenged<sup>6,22,23,30,62</sup> on the basis of high-fidelity preservation and the absence of expected taphonomic evidence like swing marks (cf. McKean et al. and Jensen et al.<sup>38,63</sup>). The orientation of rangeomorph and arboreomorph fronds orthogonal to the inferred paleoslope,<sup>30,62,64</sup> or even against the inferred paleocurrent direction (e.g., *Bradgatia* sp.; Flude et al.<sup>65</sup>), is incompatible with the dynamics of density flow events<sup>30</sup> but is consistent with the epifaunal growth of reclining taxa on hiatal surfaces beneath a turbulent clear-water current prior to the more violent ash-rich turbidity current events that smothered and preserved the fronds.<sup>22,30</sup>

Previous literature has documented random orientations of *Fractofusus* in populations from Bristy Cove, the “E” Surface at Mistaken Point, and the Johnson/H14 surface at Discovery Global Geopark.<sup>17,21,39,40</sup> However, these studies have failed to consider rheotropic growth or have inferred unrealistic turbidity current dynamics (discussed in Pérez-Pinedo et al.<sup>22</sup>). Our previous work from the Capelin Gulch site<sup>22</sup> has used an integrated approach, combining physical sedimentological evidence for paleocurrent direction in the form of current ripple trends and a novel statistical approach based on modified polythetic and monothetic clustering techniques including circular and quantitative variables. Pérez-Pinedo et al.<sup>22</sup> have interpreted the multimodal orientation trends oblique to the observed southeasterly paleocurrent as the result of rheotropic growth. The distinctive morphology and preferential orientation of *F. misrai*<sup>22</sup> suggest a trade-off between mechanical stability and feeding efficiency (cf. Darroch et al.<sup>43</sup>). Multimodal orientation trends do not necessarily suggest stochastic orientation trends but can be the result of rheotropic growth. It is critical to interpret orientation trends, together with taphonomic clues regarding life attitude, and the most parsimonious hydrodynamic interpretation.<sup>22</sup>

*Fractofusus misrai* has a low-relief fusiform body plan<sup>18,39</sup> (Figures 2 and 3) and is exclusively found in the low-energy deep marine settings of Avalonia. This contrasts with later Ediacaran taxa with broadly hemispherical morphologies, which thrived in shallow-water environments characterized by shifting currents.<sup>42,43,48</sup> Several of the deep-marine Ediacaran organisms of Avalonia are considered to have been rheotropic epibenthic organisms<sup>30</sup> growing in response to clear-water paleocurrents and oriented to maximize the efficiency of their reclining lifestyle.<sup>22</sup> Such organisms commonly dominate the intervals between the frequent density current and ashfall events that both smothered and preserved them.<sup>24,66</sup>

Current-parallel orientations of *Fractofusus* generate minor downstream eddies and consistently exhibit lower  $F_D$  across all flow velocities and size classes (Figures 4Sii and 6). High-stress areas are locally constrained, posing only a slight structural threat of current-related damage (Figure 6A). Despite current-parallel growth being the most hydrodynamic orientation, it also minimizes aspect ratio, which affects the flow experienced by the upper surface of the fossil. When *Fractofusus* is modeled in current-parallel orientations, all primary-order fronds are exposed to the same section of the water column thereby facing progressively decreasing food/oxygen concentrations and increasing concentrations of waste metabolites in the downcurrent direction<sup>22</sup> (Figure S6). However, case-dependent consideration is required since some food particles can show different inertia and the behaviors of very small particles and/or gas bubbles in the flow have not been simulated as part of this work. This is determined by the Stokes number and Archimedes number.<sup>67</sup> In contrast, non-parallel orientations would experience better flushing and increased exposure to food and oxygen, but the higher aspect ratio generates more pronounced eddying on both the lee and stoss sides, generating recirculating pulses of current against the lateral margins of the organism<sup>22</sup> (Figures 4Ti, Tiv, S4, and S5). This is demonstrated by the consistent higher  $F_D$  values simulated across all flow velocities and size classes of *Fractofusus*, and the more evenly distributed high-stress areas (Figure 6). The increased mechanical threat to non-current-parallel *Fractofusus* could have led to increased stress, lifting entire primary branches or the upstream margin of the frond. Detachment from the seafloor is possible but not demonstrated; transportation might have been terminal for *F. misrai*, but there are no transported individuals known in the Mistaken Point biotas, just partially reoriented individuals.<sup>18</sup> The *F. misrai* at the Capelin Gulch site are preferentially obliquely oriented, which likely reflects a trade-off between enhancing metabolism without compromising mechanical stability. However, it is also possible that populations that show preferential orientation trends resulted from regional paleoenvironmental controls encompassing faster flows or low nutrient availability and therefore a need to maximize feeding efficiency or reduce mechanical stress.

### Ecological role and paleobiology

*Fractofusus* is considered to have grown by both insertion of new elements and inflation of existing elements.<sup>8</sup> The large size range of individuals on some surfaces suggests that differential growth could allow *Fractofusus* to slowly respond rheotropically to assume preferential orientations.<sup>18</sup> They are not considered to have been motile and as such could not respond to changes in current orientation in any way except by growth.<sup>18</sup> Since early ontogenetic stages are not preserved at the Capelin Gulch site,<sup>22</sup> it is not possible to address such issues quantitatively. Juveniles with less than eight pairs of first-order branches are rare, suggesting that they had a lifestyle that in some way hindered their preservation.<sup>18</sup>

*Fractofusus* is commonly the most abundant fossil organism on fossiliferous surfaces in the Ediacaran of Newfoundland, which may partially be due to its capacity for continuous asexual reproduction.<sup>21,22,41</sup> This sets it apart from other less abundant rangeomorphs, which may have had other modes of reproduction.<sup>68</sup> Even our low-relief three-dimensional reconstruction of *F. misrai*<sup>18</sup> (Figure 3) which is flatter than previous interpretations<sup>17,69</sup> creates a wake of decreased current velocity that extended over two meters downstream of the organism (Figure 4). This zone of decreased flow likely altered conditions in the benthic boundary layer, potentially impacting all species living in its wake,

particularly small or juvenile organisms. We have suggested that the background clear-water current at Capelin Gulch was similar to that at Mistaken Point,<sup>24,30</sup> estimated at approximately 0.05–0.1 m/s, based on comparisons with measurements from modern offshore shelf to slope settings.<sup>70</sup> Any further reduction in the flow velocity below 0.05 m/s is likely to have led to sedimentation of fine-grained material (including POM), potentially making the seafloor more habitable. Consequently, the presence of current-slowing organisms on the seafloor leads to the baffling of bypassing sediment, where alterations in sediment rates contribute to making the seafloor more hospitable for subsequent generations (cf. Miatta et al.<sup>71</sup>).

## Conclusion

CFD is a powerful tool that has been effectively used to address aspects of the paleobiology of several Ediacaran organisms.<sup>42–45,48,49</sup> However, previous studies have not attempted to study the complex rangeomorph anatomies beyond the first order of branching.<sup>45</sup> In this work, we present the first approach to the hydrodynamics of *F. misrai* using a highly detailed morphological reconstruction with respect to three orders of rangeomorph branching on the upper surface and geometries supported by taphonomic evidence<sup>18</sup> and consistent with statistical orientation clusters determined from the field.<sup>22</sup> This has revealed some new insights into the paleobiology of *F. misrai*.

- (1) Rangeomorph branching at the secondary and tertiary order both funnels and slows currents on the surface of *F. misrai* (Figure 5). The oblique frond orientations determined from the Melrose Surface at Capelin Gulch<sup>22</sup> show an even distribution of slowed flow over the upper surface of the organism. The upper surface could thus be an adaptation to increase the efficiency of 1) collecting fine POM, 2) direct absorption of DOM, 3) direct absorption of oxygen from the entire upper surface, and 4) flushing of waste metabolites.<sup>31</sup>
- (2) Organism orientation and rheotropism relative the paleocurrent direction control the amount of drag experienced by *Fractofusus*. Given the degree of scatter, and the lack of a basal attachment, sessile reclining *Fractofusus* were likely to have been able to orientate themselves by progressively growing into the rheotropically desirable orientation. The preferred oblique bimodal orientation trends and the lack of evidence for passive or active mobility suggest that *F. misrai* at the Capelin Gulch site responded to changes in current orientation by growth rather than being passively aligned by the current (cf. Ivantsov and Paterson et al.<sup>72,73</sup>). Progressively perpendicular orientations show increasing  $F_D$  values and eddying on the lee side of the organism which could have led to structural damage, mechanical tension, and eventual lifting of individual branches as evidenced by taphonomic clues, or even terminal detachment from the seafloor (Figures 4 and 6). The preferential orientation of *F. misrai* previously documented at the Capelin Gulch site<sup>22</sup> can be explained as a compromise between maximizing exposure to the current without experiencing excessive drag. *Fractofusus* had the potential to grow in a manner that maximized aspect ratio, accessing an increased volume of unexploited water, while maintaining mechanical integrity through reduced drag. If drag was too great, then the organism would have been removed by the current; if the aspect ratio is too low, then the feeding/flushing efficiency of the organism would be compromised (Figure S6). Additionally, the wake generated downstream of the *F. misrai* hints at its potential to entrap bypassing sediment, altering the conditions in the benthic boundary layer, and sedimentation rates in its lee, especially organic particle deposition which may have benefitted organisms downstream of it (Figure 4). The assemblages of *Fractofusus*, and other reclining taxa, on other fossil-rich Ediacaran surfaces should be studied to assess the utility of our findings in better understanding the ecology and paleobiology of Ediacaran epibenthic taxa.

## Limitations of the study

This study presents certain simplifications toward natural conditions such as smooth bottom boundaries, as opposed to real textured surfaces; rigid non-mobile geometries; and individual specimen simulations. The hydrodynamics of entire *Fractofusus* communities, which would be expected from real fossiliferous surfaces, has not yet been tested due to the high computational demands. Fluid-structure interactions (FSIs) would allow mechanical deformation of organism reconstructions. It is possible that these organisms were deformed by the paleocurrents. These simplifications were implemented to reduce the computational cost of the simulations. Future research should incorporate dynamic mechanical deformation of fossil geometries and CFD-discrete element method (DEM) coupling. The behaviors of very small particles have not been simulated as part of this work because of the active nature of particle collection by organisms with—for example—choanocytes being more complex than simple consideration of flow strengths and settling.

## STAR★METHODS

Detailed methods are provided in the online version of this paper and include the following:

- KEY RESOURCES TABLE
- RESOURCE AVAILABILITY
  - Lead contact
  - Materials availability
  - Data and code availability
- METHOD DETAILS
  - Material and digital geometry
  - Computational fluid dynamics (CFD)
- QUANTIFICATION AND STATISTICAL ANALYSIS

## SUPPLEMENTAL INFORMATION

Supplemental information can be found online at <https://doi.org/10.1016/j.isci.2024.110107>.

## ACKNOWLEDGMENTS

We acknowledge the support from J. Peláez García, B. Colbourne, R. Hiscott, A. Hay, R. Taylor, E and N. Samson, and the Discovery UNESCO Global Geopark. We also acknowledge the constructive criticism by the six reviewers. Fieldwork and fossil casting in Newfoundland were conducted under permit from the Parks and Natural Areas Division of the Government of Newfoundland and Labrador. This project was supported by a Discovery Grant #RGPIN-2018-04880 from the Natural Sciences and Engineering Research Council of Canada to D.M.

## AUTHOR CONTRIBUTIONS

Conceptualization, D.P.-P., R.N., J.M.N., and D.M.; methodology, D.P.-P. and R.N.; formal analysis, D.P.-P.; investigation, D.P.-P., J.M.N., and D.M.; writing, D.P.-P. and D.M.; review and editing, D.P.-P., J.M.N., and D.M.; funding acquisition, D.M.

## DECLARATION OF INTERESTS

The authors declare no competing interests.

Received: November 21, 2023

Revised: March 10, 2024

Accepted: May 23, 2024

Published: May 24, 2024

## REFERENCES

- Waggoner, B. (2003). The Ediacaran biotas in space and time. *Integr. Comp. Biol.* 43, 104–113. <https://doi.org/10.1093/icb/43.1.104>.
- Narbonne, G.M. (2005). The Ediacara biota: Neoproterozoic origin of animals and their ecosystems. *Annu. Rev. Earth Planet Sci.* 33, 421–442. <https://doi.org/10.1146/annurev.earth.33.092203.122519>.
- Hofmann, H.J., O'Brien, S.J., and King, A.F. (2008). Ediacaran biota on Bonavista Peninsula, Newfoundland, Canada. *J. Paleontol.* 82, 1–36. <https://doi.org/10.1666/06-087.1>.
- Liu, A.G., Kenchington, C.G., and Mitchell, E.G. (2015). Remarkable insights into the paleoecology of the Avalonian Ediacaran macrobiota. *Gondwana Res.* 27, 1355–1380. <https://doi.org/10.1016/j.gr.2014.11.002>.
- Matthews, J.J., Liu, A.G., Yang, C., Mcllroy, D., Levell, B., and Condon, D.J. (2021). A chronostratigraphic framework for the rise of the Ediacaran macrobiota: new constraints from Mistaken Point Ecological Reserve, Newfoundland. *Geol. Soc. Am. Bull.* 133, 612–624. <https://doi.org/10.1130/B35646.1>.
- Mcllroy, D., Dufour, S.C., Taylor, R., and Nicholls, R. (2021). The role of symbiosis in the first colonization of the seafloor by macrobiota: Insights from the oldest Ediacaran biota (Newfoundland, Canada). *Biosystems* 205, 104413. <https://doi.org/10.1016/j.biosystems.2021.104413>.
- Noble, S.R., Condon, D.J., Carney, J.N., Wilby, P.R., Pharaoh, T.C., and Ford, T.D. (2015). U-pb Geochronology and Global Context of the Charnian Supergroup, UK: Constraints on the Age of Key Ediacaran Fossil Assemblages. *Geol. Soc. Am. Bull.* 127, 250–265. <https://doi.org/10.1130/B31013.1>.
- Brasier, M.D., Antcliffe, J.B., and Liu, A.G. (2012). The architecture of Ediacaran fronds. *Paleontology* 55, 1105–1124. <https://doi.org/10.1111/j.1475-4983.2012.01164.x>.
- Xiao, S., and Laflamme, M. (2009). On the eve of animal radiation: phylogeny, ecology, and evolution of the Ediacara biota. *Trends Ecol. Evol.* 24, 31–40. <https://doi.org/10.1016/j.tree.2008.07.015>.
- Budd, G.E., and Jensen, S. (2017). The origin of the animals and a 'Savannah' hypothesis for early bilaterian evolution. *Biol. Rev.* 92, 446–473. <https://doi.org/10.1111/brv.12239>.
- Dunn, F.S., Liu, A.G., and Donoghue, P.C.J. (2018). Ediacaran developmental biology. *Biol. Rev.* 93, 914–932. <https://doi.org/10.1111/brv.12379>.
- Dunn, F.S., Liu, A.G., Grazhdankin, D.V., Vixseboxse, P., Flannery-Sutherland, J., Green, E., Harris, S., Wilby, P.R., and Donoghue, P.C.J. (2021). The developmental biology of Charnia and the eumetazoan affinity of the Ediacaran rangeomorphs. *Sci. Adv.* 7, eabe0291. <https://doi.org/10.1126/sciadv.abe0291>.
- Laflamme, M., Xiao, S., and Kowalewski, M. (2009). From the Cover: Osmotrophy in modular Ediacara organisms. *Proc. Natl. Acad. Sci. USA* 106, 14438–14443. <https://doi.org/10.1073/pnas.0904836106>.
- Jenkins, R.J.F. (1985). The enigmatic Ediacaran (late Precambrian) genus *Rangaea* and related forms. *Paleobiology* 11, 336–355. <https://doi.org/10.1017/S0094837300011635>.
- Hoyal Cuthill, J.F., and Conway Morris, S. (2014). Fractal branching organizations of Ediacaran rangeomorph fronds reveal a lost Proterozoic body plan. *Proc. Natl. Acad. Sci. USA* 111, 13122–13126. <https://doi.org/10.1073/pnas.1408542111>.
- Anderson, M.M., and Misra, S.B. (1968). Fossils found in the Pre-Cambrian Conception Group of South-eastern Newfoundland. *Nature* 220, 680–681. <https://doi.org/10.1038/220680a0>.
- Gehling, J.G., and Narbonne, G.M. (2007). Spindle-shaped Ediacara fossils from the Mistaken Point assemblage, Avalon Zone, Newfoundland. *Can. J. Earth Sci.* 44, 367–387. <https://doi.org/10.1139/E07-003>.
- Taylor, R.S., Nicholls, R., Neville, J.M., and Mcllroy, D. (2023). Morphological variation in the rangeomorph organism *Fractofusus misrai* from the Ediacaran of Newfoundland, Canada. *Geol. Mag.* 160, 146–166. <https://doi.org/10.1017/S0016756822000723>.
- Narbonne, G.M., Laflamme, M., Trusler, P.W., Dalrymple, R.W., and Greentree, C. (2014). Deep-water Ediacaran fossils from northwestern Canada: taphonomy, ecology, and evolution. *J. Paleontol.* 88, 207–223. <https://doi.org/10.1666/13-053>.
- Clapham, M.E., Narbonne, G.M., and Gehling, J.G. (2003). Paleoeology of the oldest known animal communities: Ediacaran assemblages at Mistaken Point, Newfoundland. *Paleobiology* 29, 527–544. [https://doi.org/10.1666/0094-8373\(2003\)029<0527:POTOKA>2.0.CO;2](https://doi.org/10.1666/0094-8373(2003)029<0527:POTOKA>2.0.CO;2).
- Mitchell, E.G., Kenchington, C.G., Liu, A.G., Matthews, J.J., and Butterfield, N.J. (2015). Reconstructing the reproductive mode of an Ediacaran macro-organism. *Nature* 524, 343–346. <https://doi.org/10.1038/nature14646>.
- Pérez-Pinedo, D., Neville, J.M., Pasinetti, G., McKean, C., Taylor, R., and Mcllroy, D. (2023). Frond orientations with independent current indicators demonstrate the reclining rheotropic mode of life of several Ediacaran rangeomorph taxa. *Paleobiology* 49, 471–492. <https://doi.org/10.1017/pab.2023.2>.
- Seilacher, A. (1992). Vendobionta and Psammocorallia: lost constructions of Precambrian evolution. *J. Geol. Soc. London* 149, 607–613. <https://doi.org/10.1144/gsjgs.149.4.0607>.
- Wood, D.A., Dalrymple, R.W., Narbonne, G.M., Gehling, J.G., and Clapham, M.E. (2003). Paleoenvironmental analysis of the late Neoproterozoic Mistaken Point and Trepassey Formations, Southeastern

- Newfoundland. *Can. J. Earth Sci.* 40, 1375–1391. <https://doi.org/10.1139/e03-048>.
25. O'Brien, S.J., and King, A.F. (2005). Late Neoproterozoic (Ediacaran) Stratigraphy of Avalon Zone Sedimentary Rocks, Bonavista Peninsula, Newfoundland. *Current Research, 5* (Newfoundland and Labrador Department of Natural Resources Geological Survey), pp. 101–113.
  26. Glaessner, M.F. (1984). *The Dawn of Animal Life: A Biohistorical Study* (Cambridge University Press).
  27. Clapham, M.E., and Narbonne, G.M. (2002). Ediacaran epifaunal tiering. *Geology* 30, 627–630. [https://doi.org/10.1130/0091-7613\(2002\)030<0627:EET>2.0.CO;2](https://doi.org/10.1130/0091-7613(2002)030<0627:EET>2.0.CO;2).
  28. Antcliffe, J.B., and Brasier, M.D. (2007). *Charnia* and sea pens are poles apart. *J. Geol. Soc.* 164, 49–51. <https://doi.org/10.1144/0016-76492006-080>.
  29. Fakhræe, M., Tarhan, L.G., Planavsky, N.J., and Reinhard, C.T. (2021). A largely invariant marine dissolved organic carbon reservoir across Earth's history. *Proc. Natl. Acad. Sci. USA* 118, e2103511118. <https://doi.org/10.1073/pnas.2103511118>.
  30. McIlroy, D., Pérez-Pinedo, D., Pasinetti, G., McKean, C., Taylor, R., and Hiscott, R. (2022). Rheotropic epifaunal growth, not felling by density currents, is responsible for many Ediacaran fossil orientations at Mistaken Point. *Front. Earth Sci.* 10, 1–5. <https://doi.org/10.3389/feart.2022.849194>.
  31. Dufour, S.C., and McIlroy, D. (2017). Ediacaran pre-placozoan diploblasts in the Avalonian biota: the role of chemosynthesis in the evolution of early animal life. *Geol. Soc. Spec. Publ.* 448, 211–219. <https://doi.org/10.1144/sp448.5>.
  32. Taylor, R.S., Matthews, J.J., Nicholls, R., and McIlroy, D. (2021). A re-assessment of the taxonomy, palaeobiology and taphonomy of the rangeomorph organism *Hapsidophyllas flexibilis* from the Ediacaran of Newfoundland, Canada. *PalZ* 95, 187–207. <https://doi.org/10.1007/s12542-020-00537-4>.
  33. Pérez-Pinedo, D., McKean, C., Taylor, R., Nicholls, R., and McIlroy, D. (2022). *Charniodiscus* and *Arborea* are separate genera within the *Arboreomorpha*: Using the holotype of *C. concentricus* to resolve a taphonomic/taxonomic tangle. *Front. Earth Sci.* 9, 785929. <https://doi.org/10.3389/feart.2021.785929>.
  34. Narbonne, G.M. (2004). Modular construction of early Ediacaran complex life forms. *Science* 305, 1141–1144. <https://doi.org/10.1126/science.1099727>.
  35. Vickers-Rich, P., Ivantsov, A.Y., Trusler, P.W., Narbonne, G.M., Hall, M., Wilson, S.A., Greentree, C., Fedonkin, M.A., Elliott, D.A., Hoffmann, K.H., and Schneider, G.I.C. (2013). Reconstructing *Rangaea*: new discoveries from the Ediacaran of southern Namibia. *J. Paleontol.* 87, 1–15. <https://doi.org/10.1666/12-074R.1>.
  36. Brasier, M.D., Liu, A.G., Menon, L., Matthews, J.J., McIlroy, D., and Wacey, D. (2013). Explaining the exceptional preservation of Ediacaran rangeomorphs from Spaniard's Bay, Newfoundland: a hydraulic model. *Precambrian Res.* 231, 122–135. <https://doi.org/10.1016/j.precamres.2013.03.013>.
  37. Sharp, A.C., Evans, A.R., Wilson, S., and Vickers-Rich, P. (2017). First non-destructive internal imaging of *Rangaea*, an icon of complex Ediacaran life. *Precambrian Res.* 299, 303–308. <https://doi.org/10.1016/j.precamres.2017.07.023>.
  38. McKean, C., Taylor, R.S., and McIlroy, D. (2023). New taphonomic and sedimentological insights into the preservation of high-relief Ediacaran fossils at Upper Island Cove, Newfoundland. *Lethaia* 56, 1–17. <https://doi.org/10.18261/let.56.4.2>.
  39. Seilacher, A. (1999). Biomat-related lifestyles in the Precambrian. *Palaios* 14, 86–93. <https://doi.org/10.2307/3515363>.
  40. Vixseboxse, P.B., Kenchington, C.G., Dunn, F.S., and Mitchell, E.G. (2021). Orientations of Mistaken Point fronds indicate morphology impacted ability to survive turbulence. *Front. Earth Sci.* 9, 762824. <https://doi.org/10.3389/feart.2021.762824>.
  41. Darroch, S.A.F., Laflamme, M., and Clapham, M.E. (2013). Population structure of the oldest known macroscopic communities from Mistaken Point, Newfoundland. *Paleobiology* 39, 591–608. <https://doi.org/10.1666/12051>.
  42. Rahman, I.A., Darroch, S.A.F., Racicot, R.A., and Laflamme, M. (2015). Suspension feeding in the enigmatic Ediacaran organism *Tribrachidium* demonstrates complexity of Neoproterozoic ecosystems. *Sci. Adv.* 1, e1500800. <https://doi.org/10.1126/sciadv.1500800>.
  43. Darroch, S.A.F., Rahman, I.A., Gibson, B., Racicot, R.A., and Laflamme, M. (2017). Inference of facultative mobility in the enigmatic Ediacaran organism *Parvancorina*. *Biol. Lett.* 13, 20170033. <https://doi.org/10.1098/rsbl.2017.0033>.
  44. Darroch, S.A.F., Gibson, B.M., Syversen, M., Rahman, I.A., Racicot, R.A., Dunn, F.S., Gutarra, S., Schindler, E., Wehrmann, A., and Laflamme, M. (2022). The life and times of *Pteridium simplex*. *Paleobiology* 48, 527–556. <https://doi.org/10.1017/pab.2022.2>.
  45. Darroch, S.A.F., Gutarra, S., Masaki, H., Oлару, A., Gibson, B.M., Dunn, F.S., Mitchell, E.G., Racicot, R.A., Burzynski, G., and Rahman, I.A. (2023). The rangeomorph *Pectinifrons abyssalis*: Hydrodynamic function at the dawn of animal life. *iScience* 26, 105989. <https://doi.org/10.1016/j.isci.2023.105989>.
  46. Gibson, B.M., Rahman, I.A., Maloney, K.M., Racicot, R.A., Mocke, H., Laflamme, M., and Darroch, S.A.F. (2019). Gregarious suspension feeding in a modular Ediacaran organism. *Sci. Adv.* 5, eaaw0260. <https://doi.org/10.1126/sciadv.aaw0260>.
  47. Gibson, B.M., Darroch, S.A., Maloney, K.M., and Laflamme, M. (2021). The importance of size and location within gregarious populations of *Ernietta plateauensis*. *Front. Earth Sci.* 9, 749150. <https://doi.org/10.3389/feart.2021.749150>.
  48. Cracknell, K., García-Bellido, D.C., Gehling, J.G., Ankor, M.J., Darroch, S.A.F., and Rahman, I.A. (2021). Pentaradial eukaryote suggests expansion of suspension feeding in White Sea aged Ediacaran communities. *Sci. Rep.* 11, 4121. <https://doi.org/10.1038/s41598-021-83452-1>.
  49. Liu, P., Zhang, Y., Yang, X., Wang, B., Zhang, T., Sun, J., Tang, Q., He, K., Hao, W., Yue, N., et al. (2022). Hydrodynamic simulations of millimeter-scale Cambrian sedimentary medusozoans. *J. Geophys. Res. Biogeosciences* 127, e2022JG006854. <https://doi.org/10.1029/2022JG006854>.
  50. Gibson, B.M., Furbish, D.J., Rahman, I.A., Schmeckle, M.W., Laflamme, M., and Darroch, S.A.F. (2021). Ancient life and moving fluids. *Biol. Rev.* 96, 129–152. <https://doi.org/10.1111/brv.12649>.
  51. Mrokowska, M.M. (2020). Influence of pycnocline on settling behaviour of non-spherical particle and wake evolution. *Sci. Rep.* 10, 20595. <https://doi.org/10.1038/s41598-020-77682-y>.
  52. Dufour, S.C., and McIlroy, D. (2018). An Ediacaran pre-placozoan alternative to the pre-sponge route towards the Cambrian explosion of animal life: a comment on Cavalier-Smith 2017. *Phil. Trans. R. Soc. B.* 373, 20170148. <https://doi.org/10.1098/rstb.2017.0148>.
  53. Cavalier-Smith, T. (2017). Origin of animal multicellularity: precursors, causes, consequences—the choanoflagellate/sponge transition, neurogenesis and the Cambrian explosion. *Phil. Trans. R. Soc. B.* 372, 20150476. <https://doi.org/10.1098/rstb.2015.0476>.
  54. Butterfield, N.J. (2022). Constructional and functional anatomy of Ediacaran rangeomorphs. *Geol. Mag.* 159, 1148–1159. <https://doi.org/10.1017/S0016756820000734>.
  55. Ghisalberti, M., Gold, D.A., Laflamme, M., Clapham, M.E., Narbonne, G.M., Summons, R.E., Johnston, D.T., and Jacobs, D.K. (2014). Canopy flow analysis reveals the advantage of size in the oldest communities of multicellular eukaryotes. *Curr. Biol.* 24, 305–309. <https://doi.org/10.1016/j.cub.2013.12.017>.
  56. Singer, A., Plotnick, R., and Laflamme, M. (2012). Experimental fluid mechanics of an Ediacaran frond. *Palaeontol. Electron.* 15, 1–14. <https://doi.org/10.26879/297>.
  57. Johnston, D.T., Poulton, S.W., Goldberg, T., Sergeev, V.N., Podkovyrov, V., Vorob'eva, N.G., Bekker, A., and Knoll, A.H. (2012). Late Ediacaran redox stability and metazoan evolution. *Earth Planet Sci. Lett.* 335–336, 25–35. <https://doi.org/10.1016/j.epsl.2012.05.010>.
  58. Jensen, S. (2003). The Proterozoic and earliest Cambrian trace fossil record: patterns, problems, and perspectives. *Integr. Comp. Biol.* 43, 219–228. <https://doi.org/10.1093/icb/43.1.219>.
  59. McIlroy, D., and Logan, G.A. (1999). The impact of bioturbation on infaunal ecology and evolution during the Proterozoic-Cambrian transition. *Palaios* 14, 58–72. <https://doi.org/10.2307/3515361>.
  60. Zanzerl, H., Salvo, F., Jones, S.W., and Dufour, S.C. (2019). Feeding strategies in symbiotic and asymbiotic thyasirid bivalves. *J. Sea Res.* 145, 16–23. <https://doi.org/10.1016/j.seares.2018.12.005>.
  61. Laflamme, M., Narbonne, G.M., Greentree, C., and Anderson, M.M. (2007). Morphology and taphonomy of an Ediacaran frond: *Charnia* from the Avalon Peninsula of Newfoundland. *Geol. Soc. Spec. Publ.* 286, 237–257. <https://doi.org/10.1144/SP286.17>.
  62. McIlroy, D., Hawco, J., McKean, C., Nicholls, R., Pasinetti, G., and Taylor, R. (2020). Palaeobiology of the reclining rangeomorph *Beothukis* from the Ediacaran Mistaken Point Formation of southeastern Newfoundland. *Geol. Mag.* 159, 1160–1174. <https://doi.org/10.1017/S0016756820000941>.
  63. Jensen, S., Högstöm, A., Almond, J., Taylor, W.L., Meinhold, G., Høyberget, M., Ebbestad, J.O.R., Agić, H., and Palacios, T. (2018). Scratch circles from the Ediacaran and Cambrian of Arctic Norway and southern Africa, with a review of scratch circle occurrences. *Bull. Geosci.* 93, 287–304. <https://doi.org/10.3140/bull.geosci.1685>.

64. Hawco, J.B., Kenchington, C.G., Taylor, R.S., and Mclroy, D. (2020). A multivariate statistical analysis of the Ediacaran rangeomorph taxa *Beothukis* and *Culmofrons*. *Palaios* 35, 495–511. <https://doi.org/10.2110/palio.2020.049>.
65. Flude, L.I., and Narbonne, G.M. (2008). Taphonomy and ontogeny of a multibranching Ediacaran fossil: *Bradgatia* from the Avalon Peninsula of Newfoundland. *Can. J. Earth Sci.* 45, 1095–1109. <https://doi.org/10.1139/E08-057>.
66. Ichaso, A.A., Dalrymple, R.W., and Narbonne, G.M. (2007). Paleoenvironmental and basin analysis of the late Neoproterozoic (Ediacaran) Upper Conception and St. John's Groups, West Conception Bay, Newfoundland. *Can. J. Earth Sci.* 44, 25–41. <https://doi.org/10.1139/e06-098>.
67. Garg, R., Galvin, J., Li, T., and Pannala, S. (2012). Documentation of open-source MFiX-DEM software for gas–solids flows. [https://mfix.netl.doe.gov/download/mfix/mfix\\_current\\_documentation/dem\\_doc\\_2012-1.pdf](https://mfix.netl.doe.gov/download/mfix/mfix_current_documentation/dem_doc_2012-1.pdf).
68. Pasinetti, G., and Mclroy, D. (2023). Palaeobiology and taphonomy of the rangeomorph *Culmofrons plumosa*. *Palaeontology* 66, e12671. <https://doi.org/10.1111/pala.12671>.
69. Mitchell, E.G., and Kenchington, C.G. (2018). The utility of height for the Ediacaran organisms of Mistaken Point. *Nat. Ecol. Evol.* 2, 1218–1222. <https://doi.org/10.1038/s41559-018-0591-6>.
70. Fowler, W.A. (2014). *Boundary Layer Velocity Structure in a Coldwater Coral Area of Haddock Channel, Southwest Grand Banks*. Doctoral dissertation (Memorial University of Newfoundland).
71. Miatta, M., and Snelgrove, P.V. (2022). Sea pens as indicators of macrofaunal communities in deep-sea sediments: Evidence from the Laurentian Channel Marine Protected Area. *Deep-Sea Res. I.* 182, 103702. <https://doi.org/10.1016/j.dsr.2022.103702>.
72. Ivantsov, A.Y. (2013). Trace fossils of Precambrian metazoans “Vendobionta” and “Mollusks”. *Stratigr. Geol. Correl.* 21, 252–264. <https://doi.org/10.1134/S0869593813030039>.
73. Paterson, J.R., Gehling, J.G., Droser, M.L., and Bicknell, R.D.C. (2017). Rheotaxis in the Ediacaran epibenthic organism *Parvancorina* from South Australia. *Sci. Rep.* 7, 45539. <https://doi.org/10.1038/srep45539>.
74. Liu, A.G., Mclroy, D., Antcliffe, J.B., and Brasier, M.D. (2011). Effaced preservation in the Ediacara biota and its implications for the early microfossil record. *Palaeontology* 54, 607–630. <https://doi.org/10.1111/j.1475-4983.2010.01024.x>.
75. Mclroy, D., Brasier, M.D., and Lang, A.S. (2009). Smothering of microbial mats by macrobiota: implications for the Ediacara biota. *J. Geol. Soc.* 166, 1117–1121. <https://doi.org/10.1144/0016-76492009-073>.
76. Shashi Menon, E. (2015). *Fluid flow in pipes*. In *Transmission Pipeline Calculations and Simulations Manual* (Gulf Professional Publishing), pp. 149–234.
77. Ansys. What is Reynolds number? <https://www.ansys.com/blog/what-is-reynolds-number>.
78. Bearman, P.W., and Harvey, J.K. (1976). Golf ball aerodynamics. *Aeronaut. Q.* 27, 112–122. <https://doi.org/10.1017/S0001925900007617>.
79. Choi, J., Jeon, W.P., and Choi, H. (2006). Mechanism of drag reduction by dimples on a sphere. *Phys. Fluids* 18, 041702. <https://doi.org/10.1063/1.2191848>.
80. Smith, C.E., Beratlis, N., Balaras, E., Squires, K., and Tsunoda, M. (2010). Numerical investigation of the flow over a golf ball in the subcritical and supercritical regimes. *Int. J. Heat Fluid Flow* 31, 262–273. <https://doi.org/10.1016/j.ijheatfluidflow.2010.01.002>.
81. McLean, S.R., and Yean, J. (1987). Velocity and stress in the deep-ocean boundary layer. *J. Phys. Oceanogr.* 17, 1356–1365. [https://doi.org/10.1175/1520-0485\(1987\)017<1356:VASITD>2.0.CO;2](https://doi.org/10.1175/1520-0485(1987)017<1356:VASITD>2.0.CO;2).
82. D'Asaro, E. (1982). Absorption of internal waves by the benthic boundary layer. *J. Phys. Oceanogr.* 12, 323–336. [https://doi.org/10.1175/1520-0485\(1982\)012<0323:AOIWB>2.0.CO;2](https://doi.org/10.1175/1520-0485(1982)012<0323:AOIWB>2.0.CO;2).
83. Cushman-Roisin, B., and Beckers, J.M. (2011). *Introduction to Geophysical Fluid Dynamics: Physical and Numerical Aspects* (Academic press).
84. Menter, F.R. (1994). Two-equation eddy-viscosity turbulence models for engineering applications. *AIAA J.* 32, 1598–1605. <https://doi.org/10.2514/3.12149>.

## STAR★METHODS

## KEY RESOURCES TABLE

REAGENT or RESOURCE	SOURCE	IDENTIFIER
Deposited data		
Digital models	This paper	<a href="https://doi.org/10.5061/dryad.fxpnvx103">https://doi.org/10.5061/dryad.fxpnvx103</a>
CFD simulation results	This paper	<a href="https://doi.org/10.5061/dryad.fxpnvx103">https://doi.org/10.5061/dryad.fxpnvx103</a>
Software and algorithms		
ZBrush	ZBrush Pixologic, Inc.	<a href="https://www.maxon.net">https://www.maxon.net</a>
Rhinoceros 3D v.7	Robert McNeel & Associates	<a href="https://www.rhino3d.com">https://www.rhino3d.com</a>
Blender v.3.4.1	The Blender Foundation	<a href="https://www.blender.org">https://www.blender.org</a>
SimScale	SimScale	<a href="https://www.simscale.com">https://www.simscale.com</a>
Paraview 5-12-0	Kitware, Inc.	<a href="https://www.paraview.org">https://www.paraview.org</a>

## RESOURCE AVAILABILITY

## Lead contact

Further information and requests for resources should be directed to and will be fulfilled by the lead contact, Daniel Pérez-Pinedo ([dperezpinedo@mun.ca](mailto:dperezpinedo@mun.ca)).

## Materials availability

This study did not generate new materials.

## Data and code availability

Digital models and CFD simulation files have been deposited at Dryad (<https://doi.org/10.5061/dryad.fxpnvx103>) and are publicly available as of the date of publication. DOIs are listed in the [key resources table](#).

This paper does not report original code.

Any additional information required to reanalyze the data reported in this paper is available from the [lead contact](#) upon request.

## METHOD DETAILS

## Material and digital geometry

The upper and lower surfaces of *F. misrai* have been considered to be identical,<sup>17,39</sup> based on specimens that were inferred to have been folded, though the same specimens have more recently been considered to be rotated (Figure 2A).<sup>18</sup> Some recent published reconstructions of *Fractofusus* spp. invoked significant biconvexity<sup>4,17</sup> and some have suggested pronounced high relief,<sup>69</sup> though without any clear supporting evidence.<sup>18,30</sup> In this study we use the geometry of *F. misrai* generated from the taphonomic studies of Taylor et al.<sup>18</sup> based on specimens from the E Surface fossil assemblage in the Mistaken Point Ecological Reserve ( $565.00 \pm 0.64$  Ma).<sup>5</sup> The reconstructed height is compatible with the organisms pivoting around a point, which is inconsistent with a more voluminous biconvex model of *Fractofusus* (Figure 3).<sup>18</sup> The primary order branches of *F. misrai* have high morphological variability and lateral independence as shown by some specimens evidencing the lifting of individual branches from the sediment surface (Figure 2B). Where primary branches are densely packed, secondary order branch tips are not preserved on the lateral margins, which suggests curvature of the primary order branch away from the organism-sediment interface (Figure 2C). This rule of logic was used to reconstruct a complete *F. misrai* (Figure 3) that is significantly thinner than previous models, with the upper surfaces of branches being concave, and with the laterally-directed secondary order branches being rather curved and abutting against each other (Figure 3). In less densely packed regions of the frond (e.g., at the tips of the primary order branches), branches may be flared and have round ended secondary order branches (Figure 2D),<sup>18</sup> except where the frond margin has been lifted by a contemporaneous current, which results in a rather straight margin to the entire frond, with truncated branch tips (Figure 2E). The lower surface of *Fractofusus* is commonly preserved in extraordinary detail (sub-mm) in the form of negative relief impressions, partly below the ambient bedding plane,<sup>31</sup> with positive ridges separating the rangeomorph elements.<sup>2,74</sup> Preservation relies on the overlying unlithified tuff collapsing and casting the underlying mudstone following decomposition of the organism.<sup>2,17,74</sup> In most specimens, the proximal portion of the primary order branches close to the longitudinal axis is preserved as a deeper negative epirelief, whereas the distal margins and the longest first-order rangeomorph units show low-relief preservation (Figures 2C; Taylor et al.<sup>18</sup>; 3A, and 3C). The distal margin of first order branches are more loosely packed and range from straight to scalloped outlines suggesting they could not have displaced underlying sediment as much as the axial region. This suggests that the organisms smothered the adjacent matground and grew at a slightly lower topographic level (cf.<sup>18,75</sup>).

The three-dimensional models of *F. misrai* were created using ZBrush Pixologic, Inc. (<https://www.maxon.net/en/zbrush>; by R. Nicholls), then post-processed using Rhinoceros 3D v.7 (<https://www.rhino3d.com>) and Blender v.3.4.1 (<https://www.blender.org>). The geometry was built as a smoothed three million polygon mesh, capturing three orders of rangeomorph branching (Figure 3). Scaling followed published fossil dimensions,<sup>18</sup> and geometries were oriented according to the statistical clusters in Pérez-Pinedo et al.<sup>22</sup> Finally, results were analyzed with the post-processing visualization engine Paraview (e.g., Figures 4, 5, and 6) (<https://www.paraview.org>). Simplified digital geometry is available from Dryad (<https://doi.org/10.5061/dryad.fxpnvx103>).

### Computational fluid dynamics (CFD)

Discretization and sensitivity tests were conducted to determine optimal mesh sizes, balancing anatomical resolution with computational efficiency (computing cores, CPU usage, Figures S1–S3) at which results are independent of the mesh size. *Fractofusus misrai* geometries, consisting of approximately 300,000 to 500,000 polygons, and the corresponding flow volume region (FVRs) were meshed using SimScale standard-finite-volume meshing algorithms with automatic sizing and a medium factor fineness. The resulting mesh consists of tetrahedral and hexahedral elements. Various mesh fineness factors and region refinements were applied around the fossil geometry to explore the ideal computational parameters (Figures 3 and S1–S3). Simulations of incompressible water flow [density ( $\rho$ )  $\approx$  1,000 kg/m<sup>3</sup>; dynamic viscosity ( $\mu$ )  $\approx$  0.001 kg/(m·s)] around the reconstructed *F. misrai* geometry were performed using CFD SimScale software (<https://www.simscale.com>). Reynold numbers (Re) were calculated based on the characteristic length of *Fractofusus* ( $L_{0.05, 0.15, 0.30}$ ) ranging from 2683 ~ 64411 (Table S1). Our flow regimes are around the turbulent transition for flows around an obstacle Re 20000.<sup>50,76,77</sup> However, it is important to note that our reconstructed fossil geometry shows a complex/rough surface which results in ‘tripped’ boundary layers leading to critical implications in Reynolds number thresholds,<sup>78–80</sup> meaning it is possible to have turbulent flows at lower Reynolds numbers. Nevertheless, the aim of this study is to simulate the turbulent hydrodynamic conditions experienced by *Fractofusus* on the seafloor during the interval prior to the sediment-laden obrution events that smothered and killed them. The clear-water inter-turbiditic background currents travelled at low velocities over vast distances interacting with the roughness of the seafloor. In doing so they could be expected to have encountered innumerable obstacles of variable shapes and sizes, including seafloor topography (pits, mounds, ripples, scours, clasts, the bodies of living and dead erect and reclining organisms, channelization, etc). That is to say that the fronds we see on the Ediacaran bedding planes were not the first obstacles that the passing current was exposed to. Even if a such a current passed over a smooth seabed for such long distances, the skin friction alone would ensure turbulence at the velocities typical of modern deep ocean settings. Direct measurements of flow at the seafloor demonstrates persistent (turbulent) currents even from the deep featureless ocean abyssal plain (e.g.,<sup>81–83</sup>). Additionally, oceanographic measurements (e.g.,<sup>81–83</sup>) provide estimates of the viscous sublayer beneath abyssal currents, based on seafloor current data, to be  $\sim$ 5 mm. *Fractofusus* and most other sources of seafloor roughness would have projected through the viscous sublayer serving to maintain turbulent conditions at the Ediacaran seafloor. Reynolds numbers associated with modern boundary layers are of order 10<sup>6</sup> to 10<sup>7</sup>. In order to simulate currents of comparable strength ( $U \sim$  10 cm/s;  $U/u_* \sim$  30–35) K-Omega Shear Stress Transport SST model<sup>84</sup> was used to solve the Reynolds-averaged Navier–Stokes (RANS) equations, with a stationary solver used to compute the steady-state solution across all simulations. This model is known to better predict flow separation patterns than most RANS models.<sup>84</sup> Additionally, theoretical laminar model simulations covering the entire spectrum of modelled sizes, velocities, and orientations were tested for comparison, though laminar flows are not expected in natural deep marine settings (Table S1). The computational domain consisted of a three-dimensional rectangular FVR, measuring 400 cm x 200 cm x 40 cm allowing fully developed flows (i.e.,<sup>45</sup>). A velocity inlet condition was fixed at the -X end (Figure 3 II) of the FVR with three different flow velocities ( $U_x =$  0.05 m/s, 0.1 m/s, 0.2 m/s) while a zero-pressure outlet boundary condition was applied on the opposite +X end (Figure 3 III). The boundaries on the sides and top featured wall slip-boundary conditions, whereas the lower boundary and the *F. misrai* geometry were assigned no-slip boundary conditions (Figure 3). Lastly, our palaeobiological reconstruction of *F. misrai* was affixed to the computational domain on the bottom boundary. The organism reconstructions were modelled in three different sizes: small (5 cm x 1.5 cm), medium (16cm x 5cm), and large (30cm x 10cm) (based on Taylor et al.<sup>18</sup>; Figures 4 and S4–S6). These were positioned in different orientations with respect to the flow: parallel (0°), and perpendicular (90°) as well as oblique (35°–52°) based on the clusters determined by Pérez-Pinedo et al.<sup>22</sup> Flow dynamics from the somewhat analogous modern cold-water coral-rich areas in southwest Grand Banks were used to characterize the background clear water, turbulent, flow regimes from the Capelin Gulch site.<sup>70</sup> The results were compared to a null model in the form of an ellipse lacking rangeomorph elements and fully merged into the bottom boundary without projecting primary branches (Figure S7).

### QUANTIFICATION AND STATISTICAL ANALYSIS

Using SimScale and Paraview, the Velocity magnitude ( $U_x$ ) and streamlines were visualized and drag forces ( $F_D$ ) were computed for each simulation by integrating pressure and skin-friction over the boundary (Figures 4, 5, and 6). The distribution of the pressures and viscous (shear) forces along the elements were integrated, all the overall forces and moments calculated. To compute  $F_D$ , the projected (frontal) area of the fossil geometries was calculated (Table S1). Due to meshing difficulties,  $F_D$  values were calculated using a small millimetre-scale base for *F. misrai* that was bound to the bottom boundary. Finally,  $F_D$  was explored by decomposing the normal force of pressure for each element of the surface mesh (Figure 6). CFD simulations results are available from Dryad (<https://doi.org/10.5061/dryad.fxpnvx103>).